NASA TECHNICAL NOTE

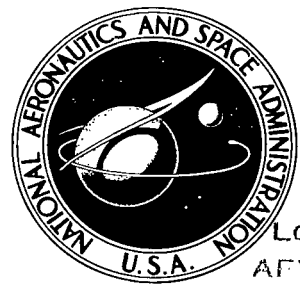

NASA TN D-8337

DESIGN STUDY OF STEADY-STATE 30-TESLA LIQUID-NEON-COOLED MAGNET

George M. Prok and Gerald V. Brown

Lewis Research Center
Cleveland, Ohio 44135

NATIONAL AERONAUTICS AND SPACE ADMINISTRATION • WASHINGTON, D. C. • NOVEMBER 1976

1. Report No. NASA TN D-8337	2. Government Accession No.
3. Recipient's Catalog No.	
4. Title and Subtitle DESIGN STUDY OF STEADY-STATE 30-TESLA LIQUID-NEON-COOLED MAGNET	5. Report Date November 1976
	6. Performing Organization Code
7. Author(s) George M. Prok and Gerald V. Brown	8. Performing Organization Report No. E-8780
	10. Work Unit No. 506-25
9. Performing Organization Name and Address Lewis Research Center National Aeronautics and Space Administration Cleveland, Ohio 44135	11. Contract or Grant No.
	13. Type of Report and Period Covered Technical Note
12. Sponsoring Agency Name and Address National Aeronautics and Space Administration Washington, D.C. 20546	14. Sponsoring Agency Code

15. Supplementary Notes

16. Abstract

A parametric study has produced a design for a 30-tesla, liquid-neon-cooled magnet that is capable of continuous operation. Cooled by nonboiling, forced-convection heat transfer to liquid neon flowing at 2.8 m^3/min in a closed, pressurized heat-transfer loop and structurally supported by a tapered structural ribbon, the tape-wound coils with a high-purity-aluminum conductor will produce over 30 teslas for 1 minute at 850 kilowatts. The magnet will have an inside diameter of 7.5 centimeters and an outside diameter of 54 centimeters. The minimum current density at design field will be 15.7 kA/cm^2.

17. Key Words (Suggested by Author(s)) Cryogenics; Cryogenic magnets; Magnet coils; Magnetic fields; Heat transfer; Cooling	18. Distribution Statement Unclassified - unlimited STAR Category 31

19. Security Classif. (of this report)	20. Security Classif. (of this page)	21. No. of Pages	22. Price*
Unclassified	Unclassified	37	$4.00

* For sale by the National Technical Information Service, Springfield, Virginia 22161

DESIGN STUDY OF STEADY-STATE 30-TESLA LIQUID-NEON-COOLED MAGNET

by George M. Prok and Gerald V. Brown

Lewis Research Center

SUMMARY

This report presents results of a design study for a 30-tesla, liquid-neon-cooled cryogenic magnet utilizing a high-purity aluminum conductor. The magnet is capable of operating in a steady state. The magnet design is based on two conceptual improvements over NASA's existing cryomagnets: (1) nonboiling, forced-convection cooling and (2) variable structural support that matches local requirements in the coils. These improvements increase the average current density by a factor of almost 4.

A parametric study was made to optimize the magnet. The goals of the optimization were to minimize power consumption, neon flow rate, magnet outer diameter, and heat flux. The optimized parameters include conductor width and thickness (6.04 and 0.180 cm, respectively), coolant channel width and thickness (0.445 and 0.038 cm, respectively), and the schedule for structural ribbon thickness, which begins at 0.070 centimeter at the inner turns, increases to 0.126 centimeter, and tapers to 0.013 centimeter at the outside of each coil. This variation in thickness gives the amount of structural support required in each part of the magnet with an approximately minimum volume of structural material. Thus, the conductor packing fraction and the average current density are as high as possible.

The magnet will have a 7.5-centimeter inner diameter and a 54-centimeter outer diameter, will required 2.8 m^3/min of coolant flow and 850 kilowatts of power, and will operate for 1 minute at peak field. The liquid neon will enter the magnet at 28 K and at a pressure of 2.8 MN/m^2 (400 psi) to suppress boiling. Seventy percent of one face of the thin, wide, high-purity-aluminum conductor will be exposed to the coolant, which flows across the conductor in thin channels. The optimized magnet is expected to produce 32.7 teslas.

INTRODUCTION

Magnetics studies at the NASA Lewis Research Center have included the design, construction, testing, and use of high-field electromagnets (refs. 1 to 6) with water-cooled copper, liquid-neon-cooled aluminum, and superconducting windings. The maximum field produced by any of these electromagnets is 20 teslas. The magnets are used for research in magnetohydrodynamic (MHD) power generation, plasma physics, and solid-state physics. In the solid-state area, still higher fields, of the order of perhaps 30 teslas, are desirable. A study in reference 7 suggests that construction of a 30-tesla cryogenic magnet should be possible with tape-wound coils of very high-purity aluminum. With sufficient refrigeration capacity, such a cryogenic magnet could be run continuously. A 30-tesla pulsed magnet (10-sec pulse) constructed of water-cooled copper has been tested at the Australian National University (refs. 8 to 10).

Existing Lewis cryogenic magnets have a maximum operating current density of about 6 kA/cm^2 (ref. 5). These coils have a uniform-thickness structure and are cooled by nucleate pool boiling of liquid neon in moderately large channels. The average conductor packing fraction (conductor volume/total coil volume) is only 0.38. Substantial increases in current density beyond that of the existing cryogenic magnets should result if the amount of stress-bearing (load) structure is varied according to local requirements in the coils and if forced-convection cooling of the conductor is used. These changes are shown to improve the conductor packing fraction by almost a factor of 2 and the allowable conductor current density by more than a factor of 2. The average current density can thus be increased by about a factor of 4.

According to preliminary estimates, a 30-tesla coil with a 7.5-centimeter-diameter bore and a 5-centimeter-diameter experimental region might be possible with the existing power supply and neon liquefaction system.

MAGNET DESIGN

External System Constraints

The Lewis Research Center neon liquefaction facility (ref. 6) provides about 1 megawatt-minute of cooling capacity per day in the latent heat of the neon. Because 1 minute of running at peak fields is desired, the maximum permissible power dissipation into the neon is 1 megawatt. Thus, one constraint of our design was to achieve a 30-tesla magnet that can operate on less than 1 megawatt of power. Cost and ease of fabrication of the entire system were also significant considerations.

To maximize current density and packing fraction, the liquid-neon coolant is pressurized to suppress boiling in the coil. To increase heat-transfer area, the magnet has

tape-wound or "pancake" coils, each of which is spirally wrapped. The coolant absorbs heat from the magnet as sensible heat that will then be rejected from the coolant by passing it through heat exchangers that are immersed in a saturated liquid-neon bath. The outside surfaces of the heat exchangers reject the heat by nucleate boiling of the liquid neon. We assume that atmospheric pressure is maintained above the liquid-neon bath. This permits the temperature of the circulating neon coolant to approach 27 K in the heat exchanger. A low coolant temperature minimizes the resistive heating by the aluminum conductor, reduces the neon use rate, and provides maximum operating times. To further improve cooling, the magnet is designed in two separate halves; the coolant flows through a heat exchanger after removing the heat from each magnet half (fig. 1). Other flow arrangements require higher capacity flow and a much larger pump motor. The series coolant flow arrangement allows both magnet halves to operate at the same temperature. The arrangement is shown in figure 1(a) as a schematic and in figure 1(b) as a cutaway of the system. Figure 2 is an enlarged view of the magnet and pressure vessel. The direction of flow is from the magnet ends toward the center plane and then from the manifolds at the center plane to the heat exchangers. Preliminary calculations showed that a neon flow rate of 2.6 to 3.0 m^3/min (700 to 800 gal/min) would be required.

Mechanical Design

Consider a tape-wound coil with thin, wide tapes of conductor and structural material wound together (insert of fig. 2). It is desirable for the magnet turns to remain tightly packed during operation to prevent slipping or even breaking of the conductor. That is, as the stress and strain build up when the magnet is turned on, the radius of every turn should increase by the same amount. However, if each turn is to be self-supporting, this constraint leads to very thick turns, because the stress in the structure must decrease as the reciprocal of the radius. One remedy would be a set of nested coils, which permits a high stress (and a thin structural ribbon) at the inner hub of each coil. Although feasible, a nested-coil geometry is undesirable from the standpoint of fabrication, and the conductor packing fraction still decreases rapidly with radius in each coil.

If the stress in the structural ribbon is kept constant with respect to radius by appropriately varying the ribbon thickness, much less structure is needed and the conductor packing fraction increases substantially. Unfortunately, at constant stress each turn stretches in proportion to its radius and gaps can open up, especially between the inner turns. However, these gaps are not larger than 0.004 centimeter (on the radius) in the cases to be presented, and we assume that this is insufficient to allow slipping. Another problem arises in the outer windings, where the field reverses direction and

presses inward on the turns, causing substantial turn-to-turn compressive forces. In a properly tailored structure, the force between these turns will not exceed the compressive yield of the aluminum, although in this region the stress in the structure can no longer be a constant. This concept for magnet design (constant stress, wherever it is possible) appears to be feasible and lends itself to a minimum number of tape-wound coils. Consequently, the parametric study in this report is confined to this design concept.

In the tape-wound coils, each turn contains a thin, wide ribbon of pure aluminum conductor; a slightly wider structural ribbon of Inconel 718 bonded to the back of the conductor; edge strips on each side of the conductor; a thin, slotted stainless-steel ribbon (spacer ribbon) across the inside face of the conductor to form the coolant channels; and a thin sheet of polyimide insulation. The details of how these parts fit together are shown in the insert of figure 2. The thickness of the conductor is chosen so that compressive and shear stresses, which build up from the inner conductor surface to the outer, do not exceed the yield stress of the pure aluminum. The axial component of magnetic force on the conductor (due to the radial field component) must be transferred to the structural member by shear through the adhesive; the bearing area of the conductor edge is insufficient to carry this load. In the outer turns, where the radial component of magnetic force is inward, the adhesive also transfers that force to the structural backing so that the conductor does not bear too heavily inward on the lands between the coolant channels. The steel "rails" on either side of the conductor are intended to transmit most of the radial compressive forces that pass between turns, although the forces and bearing areas are such that all the radial force could pass through the aluminum without exceeding its compressive yield strength.

It is important to minimize the distance between conductors in adjacent pancakes and to have as few pancakes as possible. (The spaces between the pancakes, which contain structural and insulating materials, but no conductor, are wasteful in that they do not contribute to the field.) A practical lower limit is two coils in each half of the magnet.

ANALYSIS

Structural

In our magnet structure concept the thickness of the structural ribbon varies from turn to turn in proportion to the hoop force to be absorbed in the turn. The local average current density will thus vary inversely with the local hoop force. This force is related to the local axial field strength; but because the field cannot be accurately calculated until the entire current distribution is known, the coil must be designed by a self-consistent, iterative procedure. The equations that must be solved self-consistently

are derived as follows:

Suppose the length of the magnet to be a parameter that is fixed at first but that can be varied later to optimize the magnet. To determine the required thickness of the structural ribbon for each turn in the magnet, consider only the fields and radial forces generated at the center plane of the magnet and design the structure to resist those forces. The outboard coils will therefore be somewhat conservatively designed because the radial forces on them are smaller. The axial field (at the center plane) at the location of the n^{th} turn (out of N total turns), which has an average radius r_n, may be written

$$B_n = B(I, r_n, \{r_m\}) \qquad m = 1, N \tag{1}$$

where the function B depends on the radii of all the turns: on r_n as the field point variable and on the set $\{r_m\}$ as sources. (Assume the current I is constant for all turns. And symbols are defined in appendix A.) Various approximations to the function B are used in successive stages of the calculation. The turns are treated as if they were circular, ignoring the fact that they are spiral, except that appropriate average values are chosen for the radius of the turn and for the field strength, and so forth.

The radii of the turns are related to one another by

$$r_{n+1} = r_n + t_{Al} + t_{in} + t_c + t_n^s \tag{2}$$

where t_{Al} is the thickness of the aluminum conductor, t_{in} is the insulation thickness, t_c is the thickness of the coolant channel spacer ribbon, and t_n^s is the required thickness of the structural ribbon in the n^{th} turn. The value of t_n^s is chosen (except near the outside of the coil) such that the n^{th} turn is self-supporting; that is, the radial magnetic force is exactly balanced by the hoop tension in the structural ribbon. Thus, if the p^{th} turn is the first turn that is not totally self-supporting,

$$2B_n r_n I = 2Sw_s t_n^s \qquad n < p \tag{3}$$

where the left side is the net resolved magnetic force on one-half of the n^{th} turn and the right side is twice the hoop tension in the structural ribbon, which has width w_s and is under tensile stress S for $n < p$. The need to treat the terms separately for $n \geq p$ arises as follows: The force on the outer turns is radially inward; so it is unavoidable that, at some radial location, the independent self-support of turns must be given up. From that point outward, the turns press together and forces pass radially between the turns. If the structure is assumed to be incompressible in the radial direction, for $n \geq p$ each turn increases in radius by the same amount under load. Hence,

$$\epsilon_n r_n = \epsilon_p r_p = \frac{S_n r_p}{Y} \qquad n < p \tag{4}$$

where ϵ_n is the strain of the n^{th} turn and Y is the Young's modulus of the structure. The stress S_n in the n^{th} turn (for $n \geq p$) is $S_n = S_p r_p / r_n$. The radial equilibrium of the turns $n \geq p$ requires that the summed forces outward be equal to the summed forces inward. The value of p is smaller, therefore, than the number q of the turn where field reversal occurs; and p must be found by performing iterative calculations.

The maximum compressive force between turns occurs approximately at turn q. Note that the structure is in tension for all n even though the magnetic force is inward for $n > q$. In the region $n > q$, the structural ribbon is chosen to be as thin as possible because this reduces the value of the maximum compressive force. The radially outward magnetic force from turns $p \leq n < q$ is only partly balanced against the tension in those turns by taking the structural ribbon thickness in these turns to be only 80 percent of the thickness required for self-support. In the iterative solution, p is successively adjusted so that the remaining radial force, unabsorbed in turns $p \leq n < q$, is just absorbed in turns $n > q$ and in a small band around the magnet periphery. For $n \geq p$, take

$$t_n^s = \begin{cases} 0.8\ B(n) r_n I / S_n w_s \\ t_{min}^s \end{cases} \qquad \text{(whichever is larger)} \tag{5}$$

where t_{min}^s is the minimum thickness that the structural ribbon may have. Also in the region $n \geq p$ we introduce the radial force F_n exerted radially outward by the n^{th} semiturn on the next semiturn. Thus,

$$F_n = F_{n-1} + F_n^{mag} - F_n^s \qquad n \geq p \tag{6}$$

where the magnetic force on the n^{th} semiturn is

$$F_n^{mag} = 2B(n) r_n I \tag{7}$$

and the force exerted inward by the hoop structure is

$$F_n^s = 2 t_n w_s S_n \times 0.8 \qquad n \geq p \tag{8}$$

and

$$F_{p-1} = 0 \tag{9}$$

The last turn (n = N) passes force F_n to the retaining ring around the coil. The value of N is found in the iterative solution and is chosen so that the magnet has enough turns to produce the desired field.

To begin the iterative solution of equations (1) to (9), the field at the first turn is estimated, based on the desired field at the centroid of the magnet B_o. The hoop force on the first turn can then be calculated, and it determines the required thickness of the structural ribbon. The first-iteration estimate of the diameter, axial field, and structural thickness for the second turn can then be made. A simple algebraic approximation is used to find the axial field in the first iteration. Each successive turn is treated in the same way until the initial estimate of the magnet design is obtained. Subsequent iterations toward the final design involve the straightforward use of equations (1) to (9) and the field calculation equations.

Several different methods of calculating the axial field component at the n^{th} turn B_n are used at different stages of the iterative solution. The algebraic approximation is used in the first iteration because at first very little is known about the distribution of current in the coil. This distribution is initially unknown because t_n^s is initially unknown, and hence the radii of the turns are not known except for r_1. So, at first the magnetic field at the n^{th} turn B_n is found by noting that it differs from the field at the previous turn B_{n-1} by the field increment due to a thin solenoidal element, which is approximately

$$B_n - B_{n-1} = \frac{8\pi I}{\left(\frac{4w_{Al}^2}{\lambda_z^2} + r_n^2\right)^{1/2}} \tag{10}$$

where the axial packing fraction λ_z is four times the conductor width divided by the magnet length and where the field at the first turn is estimated. In subsequent iterations, equations (1) to (9) uniquely determine a magnet design when a more exact expression for the function B is used.

The required expressions for calculating the radial and axial field components at an arbitrary field point for a right-circular solenoid with a uniform current density are provided in reference 11. Although the current density in the present case is far from uniform, one can easily divide the coil into regions in which the variation is modest and, by using a suitable average current density for each region, sum the contributions of the regions to obtain as good an approximation as is desired. (Axial current-density variations in the conductor were neglected. Since small effects due to the neon temperature

rise are partially self-compensating, the net result is not serious.) Thus,

$$B_n = \sum_i B_i(\bar{J}_i, a_i, \alpha_i, \beta_i) \tag{11}$$

where the index i refers to the various radial regions. For the i^{th} region, $\bar{J}_i$ is the weighted average current density, a_i the inner radius of that region, α_i the ratio of outer radius to inner radius, β_i the conductor width divided by $2a_i$. The accuracy was improved with minimum computing expenditure by using a weighted average to calculate J_i rather than a simple numerical one. (A discussion of this weighted average is given in appendix B.) Thus,

$$\bar{J}_i \equiv \frac{\sum_n w_n J_n t_n}{\sum_n w_n t_n} \tag{12}$$

where the index n runs over all terms in the i^{th} region, t_n is the total thickness of the n^{th} turn, the current density in the n^{th} turn is defined as

$$J_n \equiv \frac{I\lambda_z}{t_n w_{Al}} \tag{13}$$

and the weighting factor w_n is

$$w_n \equiv \left[r_n^2 + 4\left(\frac{w_{Al}}{\lambda_z}\right)^2 \right]^{-1/2} \tag{14}$$

With this weighting factor, the field at the center of the coil, calculated by using the average current density, will be correct regardless of the radial variation of the actual density. The field in the windings, calculated by using the same weighting factor, will not be exactly correct; but the accuracy may be improved by choosing as many radial regions as desired. Considering the coil as just one region would have been nearly accurate enough for our calculation; but we used five regions, which changed the field by about 1 percent. However, the parametric studies were done with the first iteration, which gave values for all variables within a few percent of the values given by the final self-consistent solution.

Cooling

For the cooling calculation, only one-half of the magnet, which contains two pancake coils, need be considered. The other half of the magnet is simply a mirror image. However, it is necessary to distinguish between the two pancakes in one-half; and we denote them by an index m such that $m = 1$ is the coil that is further from the center plane and into which the liquid neon first enters from one of the heat exchangers. The heat transfer from conductor to liquid neon in the n^{th} turn of the m^{th} coil is described by

$$Q^{nm}_{resistive} = hA_n \Delta T_{nm} \tag{15}$$

where h is the surface-to-liquid heat-transfer coefficient, A_n is the area of the conductor that is in contact with the liquid neon, and ΔT_{nm} is the temperature difference between the conductor surface and the average bulk temperature of the liquid neon. Further,

$$Q^{nm}_{resistive} = \frac{I^2 \rho_{nm}(B_{nm}, T_{nm}) 2\pi r_n}{t_{Al} w_{Al}} \tag{16}$$

where ρ_{nm} is the resistivity of the aluminum at temperature T_{nm} and magnetic field strength B_{nm} and w_{Al} is the conductor width. Also,

$$\Delta T_{nm} = T_{nm} - T^{neon}_m \tag{17}$$

where the average bulk temperature of the neon in the m^{th} coil T^{neon}_m was determined as follows: We arbitrarily specified in the computer program the increase in neon temperature T_{rise} from magnet inlet to magnet outlet through the intermost coolant channels and calculated the required flow rate by balancing the heat produced in the first turn with the sensible heat acquired by the liquid neon. The fluid velocity V, neon temperature rise T_{rise}, and power dissipated in the innermost turn Q_{1m} are related by the heat balance

$$Q_{1m} = \rho_{Ne} C_p V w_c t_c T_{rise} \tag{18}$$

It was assumed that enough hydraulic head ΔP will be provided to produce the velocity in the innermost coolant channels V. The coolant channels in all turns are subjected to approximately the same head and will therefore have approximately the same V, but the

resistive heat dissipated varies with the turns and hence the value of the temperature rise also varies. This change in T_{rise} as a function of n was neglected and the value from equation (18) was used throughout the coil. This approximation is a conservative one and overestimates the total required cooling.

Thus, for the average neon temperature in the first coil

$$T_{n1}^{neon} = T_{inlet} + \frac{T_{rise}}{4} \tag{19a}$$

was used, and for the average neon temperature in the second coil

$$T_{n2}^{neon} = T_{inlet} + \frac{3T_{rise}}{4} \tag{19b}$$

was used, where T_{inlet} is the neon temperature at the magnet inlet and T_{rise} is one of the parameters that is ultimately chosen on the basis of several considerations to be discussed. The heat-transfer coefficient in equation (15) was calculated from a Dittus-Boelter correlation, which has been shown to correlate forced-convection, heat-transfer data for liquid neon under pressure (ref. 12). This relation between the Nusselt number Nu, the Prandtl number Pr, and the Reynolds number Re is

$$Nu = 0.023\, Re^{0.8} Pr^{0.4} \tag{20}$$

where

$$Nu = \frac{hD}{k} \tag{21}$$

$$Pr = \frac{C_p \mu}{k} \tag{22}$$

$$Re = \frac{\rho_{Ne} VD}{\mu} \tag{23}$$

D is the hydraulic diameter of a coolant passage, and μ and k are the kinematic viscosity and thermal conductivity of liquid neon, respectively, evaluated at 28 K and 2.8-MN/m^2 (400-psi) pressure. For our channels,

$$D = \frac{2t_c w_c}{t_c + w_c} \tag{24}$$

The resistivity ρ_{nm} of equation (16) depends on the aluminum temperature and on the magnetic field strength. The grade of aluminum we expect to use shows an approximate power-law dependence of resistivity on temperature T between 25 and 40 K in a zero applied field:

$$\rho(0,T) = 5.92\times10^{-14}\, T^{2.147} \tag{25}$$

The resistance in a magnetic field is taken from Coruccini (ref. 13) as

$$\rho(B,T) = \rho(0,T)\,\frac{1 + B_*^2(1 + 0.00177\, B_*)}{1.8 + 1.6\, B_* + 0.53\, B_*^2} \tag{26}$$

where

$$B_* = 0.001\, B \times \frac{\rho_{RT}}{\rho(0,T)} \tag{27}$$

and ρ_{RT} is the room-temperature resistivity of aluminum. Equations (25) and (26) can be applied to any turn if the temperature of the conductor and the field strength in the turn are known.

Equations (16) to (27) form a set of equations that were solved self-consistently by iteration on the computer to obtain the temperature of each turn, the power dissipated by each turn, and the required velocity of coolant in the channels. The total electrical power needed was found by summing the power dissipated in individual turns. The total flow rate of coolant was found from the coolant flow velocity and the number and size of the channels. Physical properties of the aluminum conductor and the neon used in this study are given in table I. Structural properties chosen are those for Inconel 718.

Local heat flux, conductor temperature, conductor resistance, magnet volume, and magnet power are all interrelated and are dependent on the coolant flow rate. To match the desired operating conditions to the existing liquid-neon facility, cryostat, and power supply, a limit of 2.8 m^3/min (750 gal/min) was imposed for the circulating pump. With this flow rate, the conductor temperature and thus the conductor resistance and power required can be kept suitably low at an imposed heat flux of 11 W/cm^2. A significant increase in conductor resistance would require more than 1 megawatt to power the magnet.

However, reference 11 shows that the liquid neon could remove more than 16 W/cm^2 if necessary. Existing cryostat electrical feedthroughs sized for 45 kiloamperes determined the maximum current.

RESULTS AND DISCUSSION

Parametric Study

Since the optimized results were well approximated by the first iteration, only these results are presented and discussed for the parametric study. Using the more exact calculations for the parametric study would only consume computer time without changing the results. However, for the final design results that are presented in table II, the more exact calculations were used.

Although 30 teslas is the minimum desired field strength, the parametric study included fields as high as 40 teslas to provide leeway for downrating the magnet if unexpected problems should arise. In determining this magnetic field, magnet safety and facility capability were primary considerations. To determine the maximum feasible magnetic field, the first phase of the study produced these near-optimum values of the program input variables:

(1) Axial packing fraction, 0.85
(2) Conductor width, 5.7 cm
(3) Conductor thickness, 0.180 cm
(4) Coolant channel thickness, 0.038 cm
(5) Coolant channel width, 0.45 cm
(6) Coolant channel spacing, 0.64 cm
(7) Neon temperature rise, 5 kelvins

Items five and six provide that 70 percent of one face of the aluminum is exposed to the coolant. The particular values chosen for coolant channel width and spacing are simply reasonable values for magnet fabrication.

Using these results, design computations for various field strengths and bore diameters were made. The conductor current was always set at 40 kiloamperes, well below the 45-kiloampere feedthrough limit. The effect of the design field on magnet power, neon flow rate, and current density for various bore diameters is shown in figures 3 to 5. A 7.62-centimeter bore diameter would accommodate a test section already in existence. Figure 3 shows that, for this bore diameter, about 37 teslas at the electrical bore is the maximum field that could be achieved at a magnet power dissipation level of 1000 kilowatts. However, larger fields can be obtained at smaller bore diameters without exceeding the 11-W/cm^2 heat flux. About 36 teslas can be obtained in a 7.62-centimeter-bore coil with the limiting flow rate of 2.85 m^3/min (fig. 4) and a 5-kelvin

temperature rise in the neon. At a bore diameter of 3.81 centimeters, almost 41 teslas could be obtained. Figure 5 shows how the current density varies with radial position in the magnet for selected design fields and bore diameters. The current density in figure 5 is the design current (40 kA) divided by the total cross-sectional area of the winding. This area includes the conductor, the insulation, the slotted stainless-steel spacer ribbon, the structural strength member, and the space between the pancakes. The variation in Inconel thickness is the reason for the change in current density. The current density varies more through the coil for large bore diameters and for large magnetic fields. Also, magnet diameter increases as the design bore diameter and the magnetic field increase. To fit this cryomagnet into the dewar of the magnetics and cryophysics facility, the magnet outside diameter must not be much more than 50 centimeters. This rules out magnets that can produce 37 teslas in a bore of 7.62 centimeters (fig. 5).

From an analysis of the results shown in figures 3 to 5, it was apparent that the parametric study should only include fields below 36 teslas at the electrical bore. This means a design magnetic field B_o of about 35 teslas at the magnet's center. To allow for various approximations made in the computer model, designing for 35 teslas gives almost a 17 percent safety factor in magnetic field for a 30-tesla magnet design. Consequently, the remainder of the study used a nominal 35 teslas as the design point to obtain a slightly conservative 30-tesla design.

Figures 6 and 7 both show the effect of conductor width and thickness on the heat flux to the liquid neon from the conductor. For a fixed current (40 kA) the Joule heating diminishes with increasing conductor cross section. Furthermore, the wider the conductor, the larger the heat-transfer area is. The resulting rapid drop in heat flux as a function of conductor width (for fixed thickness) is shown in figure 6. There it can be seen that the conductor width should be 5.71 centimeters or greater to assure a heat flux less than 11 W/cm^2. Similarly, but less strongly, figure 7 shows that the lower resistance of a thicker conductor decreases the heat flux.

The variation of the magnet power and neon flow rate required with conductor width and thickness is shown in figures 8 and 9, respectively. There is clearly no significant variation with thickness. Below a conductor width of about 5 centimeters, both magnet power and neon flow rate increase rapidly. In fact, the neon flow rate exceeds the maximum allowable rate of 2.85 m^3/min at widths less than 5 centimeters. On the other hand, the maximum magnet power and neon flow rate are essentially the same for conductor widths of 6.04 and 6.35 centimeters. It can be concluded that over the range studied, a wide and thick conductor is desirable. However, as the conductor becomes wider and thicker, the average current density decreases and the magnet diameter increases significantly (fig. 10). Although there were only small differences in performance between the 6.04- and 6.35-centimeter-wide conductors, the latter gave a sufficiently larger diameter magnet that incorporating the system into the facility dewar would result in major design problems. Consequently, the 6.04-centimeter width was

selected as the better choice. In like manner, comparing performance factors and magnet diameter suggests the best choice in thickness to be 0.18 centimeter. A composite plot of the various parameters discussed is shown in figure 11, where the parameters are plotted as a function of magnet radius and conductor current density.

Other independent variables included in this parametric study are axial packing fraction, coolant channel parameters, insulation thickness, and neon temperature rise. These will only be discussed qualitatively.

The axial packing fraction of the conductor affects the average current density; hence, it has a significant effect on neon flow rate and neon temperature rise. It should be as close to 1.00 as possible. The study shows, however, that a practical limit is 0.90 for uniformly spaced coils. This limit is dictated by the insulating radial stringers required between pancakes. However, there must be manifolds at the center plane; hence, a larger gap is required there to handle the flow. This reduces the overall axial packing fraction to 0.85, the value used in these calculations. The lower packing fraction reduces the field attained at a design neon temperature rise of 5 kelvins, but the field is still adequately greater than the desired operating field of 30 teslas. If the circulating pump in operation falls below the design flow rate, the design field can still be achieved by operating at a higher neon temperature rise. As shown by the computed values in table III, the designed magnet can operate with a 7-kelvin neon temperature rise and still have other parameters below the imposed limit discussed earlier in the report. However, the total available operating time for the magnet would be less at this greater temperature rise.

The slotted stainless-steel spacer ribbon shown in figure 2 and discussed earlier provides the passages for cooling the conductor. It was determined that for a 6-centimeter-wide conductor the openings in the slotted ribbon should permit about 70 percent of the conductor to be in contact with the neon. A smaller percentage would increase the heat flux, and a larger percentage would reduce the contact area for passing force radially between turns. Increasing the thickness of the slotted stainless-steel ribbon (and hence the coolant channel thickness) has an adverse effect on the heat transfer. A smaller thickness was considered impractical. The selection of coolant channel width and spacing was determined from various practical considerations. The values chosen for the coolant channel parameters were discussed earlier. The insulation thickness includes a 0.005-centimeter-thick polyimide insulating film and an adhesive layer no thicker than 0.01 centimeter. Choosing thinner insulation affects the other variables by less than 5 percent.

Magnet Design

Values of independent variables were chosen on the basis of the results of the first

iteration of the mechanical design. Accurate values of the dependent variables are of course obtained only after the iteration proceeds to a self-consistent final design. Nine steps were used in the iteration procedure; however, after seven steps the design was in the range of fabrication precision.

Material physical properties from table I were used in these final design calculations. The design results are shown in tables IV(a) and (b). The differences between the two designs are the result of different minimum structural thicknesses used in the computations. Near the outside of the magnet the required thickness of the Inconel structure becomes too small to permit easy handling, so a minimum thickness was imposed, as indicated in equation (5). The most important difference between the two values considered, 0.0248 and 0.0124 centimeter, is that the thicker limit requires a maximum force of 30.3 MN/m^2 (4400 psi) to be passed between turns, while the thinner limit requires only 24.6 MN/m^2 (3570 psi). The design with a minimum Inconel thickness of 0.0248 centimeter may be marginal since the turn-to-turn compressive force reaches 30.3 MN/m^2, which is approximately the compressive yield of the pure aluminum. Table III compares the operating parameters for the two designs at design and slightly off-design conditions. Comparing the two designs and the operating results shows that the design in table IV(a) is the more conservative; therefore, it was selected as the more desirable design.

An enlarged gap at the center plane of the magnet is needed to accommodate the neon flow. This larger gap reduces the maximum magnetic field to about 32.7 teslas (fig. 12). Also shown in figure 12 is the field of a magnet that has uniformly spaced coils. In both cases the axial packing fraction is 0.85; however, the magnet with uniformly spaced coils reaches a field of 35.1 teslas at the center plane. This field gradually drops off to 33.9 teslas at a distance of 5 centimeters from the center plane; then the field drops off rapidly.

The field on the axis of the designed magnet is 32.7 teslas at the center and varies less than ±1.0 percent along a 13-centimeter length (fig. 12). The experimental bore radius is 3.18 centimeters. In this bore, the radial uniformity of the axial field is at least as good as that on the axis except on and near the center plane, where the field decreases almost 3 percent (tables V(a) and (b)). Otherwise, the large center-plane gap yields a larger test volume, which means a more uniform field over a large volume than for a magnet with uniformly spaced coils. The actual separation between the conductors within each pair of coils is 0.64 centimeter. The two magnet pairs have a conductor separation distance of 2.86 centimeters, that is, 1.43 centimeters from the center plane. The location of the coils is indicated in figure 12.

The axial and radial magnetic fields within the envelope of the magnet are shown in tables V(a) and (b), respectively. The axial field in the array is positive until the 65th turn. At this point, the axial field is negative between 4 and 10 centimeters from the center plane. Negative axial fields at the center plane to 12 centimeters from the center

plane occur from the 66th to the 73rd turns. Because of the large center gap, the radial magnetic field changes sign in a region near the center plane. Beyond 6 centimeters from the center plane, the radial field has the usual sign.

Figure 13 presents the total local current densities as a function of radial position for the design in table IV(a). The radial location where turn-to-turn force passing begins is evident. Current density was constant in the last several turns of the coil because the minimum structural thickness was reached.

CONCLUSIONS

A feasible design for a cryomagnet to produce more than 30 teslas was established by a computer study. The following results and conclusions were obtained:

1. A large-bore, 30-tesla cryomagnet can be constructed to operate continuously with the power and cooling available at the Lewis Research Center magnetic and cryophysics facility. The final design gives a magnet with a uniform magnetic field over a length of 13 centimeters and a radius of 3.68 centimeters. Both axial and radial field uniformity is within ±1 percent except at the center plane, where the radial field decreases by less than 3 percent at the 3.68-centimeter radius. These results are based on the following magnet design concept:

   a. Cooling by forced-convection, liquid-neon heat transfer, with a neon temperature rise of 5 kelvins
   b. Tape-wound coil construction with a high-purity-aluminum conductor
   c. A large gap of approximately 3 centimeters between the two coils near the magnet center plane
   d. Varying thickness of the structural member according to local requirements, except near the outside of the magnet, where a minimum thickness (0.0124 cm) is imposed

2. The axial packing fraction must not be greater than 0.85 for adequate magnet cooling. A large gap between the magnet halves is required to accommodate coolant manifolds. In each half of the magnet the conductor begins 1.5 centimeters from the center plane. The separation distance between the conductors in each magnet half is 0.635 centimeter.

3. The parametric study shows that the conductor should be between 5.0 and 6.5 centimeters wide and 0.175 and 0.180 centimeter thick. This would result in a magnet radius of about 25 to 28 centimeters. The selected design gives a radius of 26.9 centimeters.

4. The selected design will have a minimum structural member thickness of 0.0124 centimeter. With a neon temperature rise of 5 kelvins, the heat flux will be 8.99 W/cm^2 and the power 854 kilowatts. With a neon temperature rise of 7 kelvins, the magnet

would still be within other operating limits. The 854 kilowatts required at the design point means the magnet would operate at 30 teslas for more than 1 minute with the Lewis neon liquefaction system.

Lewis Research Center,
National Aeronautics and Space Administration,
Cleveland, Ohio, June 22, 1976,
506-25.

APPENDIX A

SYMBOLS

A_n area of conductor in contact with neon

a_i inner radius of i^{th} region

B magnetic field strength

C_p specific heat

D hydraulic diameter

F force

f function

h heat-transfer coefficient

I current in each turn

i index to various radial regions

J current density

$\bar{J}$ weighted average current density

k thermal conductivity

m magnet "pancake" index

N total number of turns

Nu Nusselt number

n turn number index

Pr Prandtl number

p index of first not-totally-self-supporting turn

Q heat transfer or power

q turn where field reversal occurs

Re Reynolds number

r radius coordinate

S tensile stress

s structural member

T temperature

t thickness

t_{Al} thickness of aluminum conductor

t_c thickness of coolant channel spacer ribbon

t_{in} thickness of insulation

t_n^s thickness of structural ribbon in n^{th} turn

V velocity in innermost coolant channels

w_{Al} width of conductor

w_c width of coolant channel

w_s width of structural ribbon

Y Young's modulus

α nondimensional coil-radius parameter (outer radius/inner radius)

β nondimensional coil-length parameter (length/inner diameter)

ϵ strain

λ_z axial packing fraction of conductor

μ viscosity

ρ_{Ne} density of neon

ρ_{nm} aluminum resistivity

APPENDIX B

WEIGHTED AVERAGE CURRENT DENSITY

The field at the center of a thin finite solenoid of half length l and radius a is

$$B = \frac{\mu_o nI}{\left(1 + \frac{a^2}{l^2}\right)^{1/2}} \tag{B1}$$

where n is the number of turns per unit length and μ_o is the vacuum permeability. For a solenoid of radius r, incremental thickness dr, and current density J this becomes

$$dB = \frac{\mu_o J\, dr}{\left(1 + \frac{r^2}{l^2}\right)^{1/2}} \tag{B2}$$

Then for a thick solenoid, in which J may vary with r, integration gives

$$B_{J(r)} = \mu_o \int \frac{J(r)\,dr}{\left(1 + \frac{r^2}{l^2}\right)^{1/2}} \tag{B3}$$

For the special case of constant J this becomes

$$B_{J=C} = \mu_o J \int \frac{dr}{\left(1 + \frac{r^2}{l^2}\right)^{1/2}} \tag{B4}$$

Consider the following definition of a weighted average current density $\bar{J}$ with respect to

the weighting factor $\left[1 + (r^2/l^2)\right]^{1/2}$:

$$\bar{J} \equiv \frac{\int \frac{J(r)\,dr}{\left(1 + \frac{r^2}{l^2}\right)^{1/2}}}{\int \frac{dr}{\left(1 + \frac{r^2}{l^2}\right)^{1/2}}} \tag{B5}$$

Note that the current density at small values of r is weighted more heavily exactly in proportion to its effectiveness in producing a magnetic field, as can be seen from equation (B2). By using (B3) this may be rewritten as

$$B_{J(r)} = \mu_o \bar{J} \int \frac{dr}{\left(1 + \frac{r^2}{l^2}\right)^{1/2}} \tag{B6}$$

which has the same form as equation (B4) except that the constant current density J is replaced by the weighted average current density $\bar{J}$. Because the available subroutine for calculating the field is exact when the current density is uniform but cannot deal with a variable J, the weighted average current density from equation (B5) was calculated and used. The field calculated in this way is therefore exact at the solenoid center but not at other points. Subdivision of the coil into a few radial sections, for each of which an average current density was calculated, and the addition of the field contributions of the sections provided the required accuracy at all points.

The weighting factor $\left[1 + (r^2/l^2)\right]^{-1/2}$ can be put into the exact form used in the body of the paper by multiplying by l^{-1}, since the factor always appears simultaneously in the numerator and the denominator. In this report, l is equal to $2(w_{Al}/\lambda_z)$. Substituting this into equation (B5) and using summation notation yield equation (13).

REFERENCES

1. Laurence, J. C.; et al.: A Large Liquid-Neon-Cooled Electromagnet. Proceedings of the International Conference on High Magnetic Fields, Ch. 15, The MIT Press and John Wiley & Sons, Inc., 1961, pp. 170-179.

2. Laurence, James C.: High-Field Electromagnets at NASA Lewis Research Center. NASA TN D-4910, 1968.

3. Laurence, James C.; et al.: Cryogenic and Superconducting Magnets. Plasmas and Magnetic Fields in Propulsion and Power Research. NASA SP-226, 1969, pp. 143-181.

4. Laurence, James C.; and Coles, Willard D.: Design, Construction, and Performance of Cryogenically Cooled and Superconducting Electromagnets. NASA TM X-52121, 1965.

5. Brown, Gerald V.; and Coles, Willard D.: High-Field Liquid-Neon-Cooled Electromagnets. NASA TM X-52119, 1965.

6. Coles, W. D.; Laurence, J. C.; and Brown, G. V.: Cryogenic and Superconducting Magnet Research at the Lewis Research Center. NASA TM X-52627, 1969.

7. Brown, G. V.: High-Field Cryogenic Magnets with Pure Aluminum Conductor. NASA TM X-52571, 1969.

8. Cardon, P. O.: Design Principles Relating to the Strength and Structure of the ANU 30 T Electromagnet. J. Phys. E: Sci. Instru., vol. 5, 1972, pp. 654-656.

9. Cardon, P. O.: Design and Construction of the Inner Solenoid of the ANU 30 T Electromagnet. J. Phys. E: Sci. Instru., vol. 5, 1972, pp. 663-666.

10. Cardon, P. O.: Testing the ANU 30 T High Field Magnet at Canberra. J. Phys. E: Sci. Instru., vol. 5, 1972, pp. 667-668.

11. Brown, Gerald V.; and Flax, Laurence: Superposition Calculations of Thick Solenoid Fields from Semi-Infinite Solenoid Tables. NASA TN D-2494, 1964.

12. Papell, S. S.; and Hendricks, R. C.: Liquid Neon Heat Transfer as Applied to a 30-Tesla Cryomagnet. NASA TM X-71712, 1975.

13. Corruccini, R. J.: The Electrical Properties of Aluminum for Cryogenic Electromagnets. NBS TN-218, 1964.

TABLE I. - PHYSICAL PROPERTIES OF MATERIALS USED

IN COMPUTER STUDY

Aluminum:	
Resistivity at room temperature, Ω-m	2.8×10^{-8}
Resistivity at 28 K, Ω-m	4.88×10^{-11}
Residual resistivity ratio	~2000
Inconel 718:	
Yield strength, N/m^2	12.7×10^{8}
Tensile strength, N/m^2	16.8×10^{8}
Area reduction, percent	25
Elongation at 20 K, percent	30
Neon:	
Mass density, kg/m^3	1200
Viscosity, kg/m-sec	0.00012
Thermal conductivity, W/m-K	0.126
Heat capacity at constant pressure, W-sec/kg-K	1950
Heat of vaporization at 28 K, J/kg	85×10^{3}

[a]If not noted, properties are in 25 to 40 K range.

TABLE II. - FINAL MAGNET DESIGN RESULTS

(a) Input variable

Magnetic field, T	35
Conductor current, kA	40
Distance of start of conductor winding from magnet centerline, cm	3.8
Axial packing fraction	0.85
Coolant channel width, cm	0.45
Coolant channel thickness, cm	0.038
Coolant channel spacing, cm	0.64
Conductor thickness, cm	0.180
Conductor width, cm	6.04
Insulation thickness, cm	0.015
Neon inlet temperature, K	28
Rise in neon coolant temperature, kelvin	5.0

(b) Output variable

Magnet outside diameter, cm	54
Reynolds number	1.62×10^{4}
Magnet pressure drop, N/m^2	2.6×10^{4}
Magnet coolant channel heat flux, W/cm^2	8.99
Magnet power required, kW	855
Magnet neon flow rate, m^3/min	2.78
Neon use rate, m^3/min	0.49
Average conductor temperature, K	35.7
Maximum conductor temperature, K	37.0
Dynamic resistivity ratio	109

TABLE III. - COMPARISON OF MAGNET OPERATING PARAMETERS

Minimum thickness of Inconel 718 structural ribbon, cm	Neon temperature rise, kelvin	Heat flux, W/cm^2	Power, kW	Neon flow rate, m^3/min	Neon use rate, m^3/min	Magnet centerplane force, N
[a]0.0124	[a]5	8.99	854.5	2.78	0.488	2.30×10^7
	6	9.60	914.1	2.46	.522	2.30×10^7
	7	10.24	974.9	2.23	.557	2.30×10^7
[a]0.0248	[a]5	8.98	854.5	2.78	0.488	2.29×10^7
	6	9.60	914.0	2.46	.522	2.29×10^7
	7	10.23	974.7	2.23	.557	2.29×10^7

[a]Design conditions.

TABLE IV. - FINAL MAGNET DESIGN

(a) Assuming a minimum Inconel-718 structural ribbon thickness of 0.0124 centimeter

Turn	Magnetic field, T	Average turn diameter, cm	Thickness of Inconel 718 structural ribbon, cm	Length of aluminum conductor, m	Overall current density, kA/cm^2	Force received by turn, kN	Force passed by turn, kN	Turn	Magnetic field, T	Average turn diameter, cm	Thickness of Inconel 718 structural ribbon, cm	Length of aluminum conductor, m	Overall current density, kA/cm^2	Force received by turn, kN	Force passed by turn, kN
1	35.25	8.24	0.0698	0.244	18.59	0	0	41	12.85	35.6	0.0970	27.85	17.05	152.8	189.2
2	34.66	8.84	.0736	.549	18.35			42	12.35	36.2	.0968	29.00	17.06	189.2	225
3	34.06	9.45	.0775	.824	18.13			43	11.85	36.9	.0962	30.20	17.09	225	260
4	33.47	10.07	.0810	1.159	17.92			44	11.35	37.5	.0955	31.35	17.13	260	294
5	32.86	10.70	.0846	1.495	17.72			45	10.86	38.2	.0947	32.60	17.18	294	325
6	32.26	11.32	.0878	1.830	17.54			46	10.32	38.8	.0930	33.80	17.26	325	359
7	31.65	11.98	.0911	2.230	17.36			47	9.73	39.5	.0906	35.05	17.39	359	388
8	31.04	12.61	.0942	2.625	17.20			48	9.15	40.1	.0881	36.30	17.52	388	419
9	30.44	13.29	.0973	3.02	17.04			49	8.58	40.7	.0854	37.60	17.68	419	447
10	29.83	13.93	.1000	3.48	16.90			50	8.01	41.4	.0820	38.85	17.86	447	469
11	29.21	14.60	.1027	3.94	16.77			51	7.45	42.0	.0787	40.1	18.06	469	499
12	28.60	15.28	.1052	4.42	16.65			52	6.89	42.6	.0750	41.2	18.28	499	522
13	27.99	15.94	.1074	4.91	16.53			53	6.33	43.3	.0708	42.9	18.52	522	545
14	27.38	16.63	.1093	5.42	16.43			54	5.78	43.8	.0665	44.3	18.78	545	565
15	26.77	17.32	.1116	5.96	16.34			55	5.24	44.5	.0620	45.6	19.08	565	584
16	26.19	19.18	.1132	6.56	16.25			56	4.70	45.1	.0571	47.1	19.40	584	600
17	25.64	18.69	.1152	7.14	16.16			57	4.17	45.6	.0521	48.6	19.75	600	615
18	25.09	19.40	.1170	7.75	16.08			58	3.65	46.2	.0465	49.9	20.13	615	629
19	24.55	20.10	.1187	8.39	16.00			59	3.14	46.8	.0411	51.4	20.53	629	641
20	24.00	20.8	.1200	9.02	15.94			60	2.65	47.4	.0356	52.9	20.95	641	651
21	23.46	21.5	.1212	9.70	15.88			61	2.10	47.9	.0287	54.4	21.50	651	659
22	22.92	22.2	.1225	10.40	15.83			62	1.46	48.4	.0206	56.0	22.20	659	665
23	22.38	22.9	.1237	11.22	15.79			63	.85	48.9	.0124	57.5	22.92	665	668
24	21.84	23.6	.1241	11.84	15.76			64	.27	49.4		59.0		668	660
25	21.31	24.3	.1248	12.60	15.73			65	-.31	49.9		60.6		660	639
26	20.77	25.1	.1252	13.41	15.71			66	-.89	50.4		62.1		639	608
27	20.24	25.8	.1254	14.22	15.70			67	-1.48	50.8		63.7		608	566
28	19.71	26.5	.1256	15.02	15.69			68	-2.06	51.3		65.4		566	509
29	19.18	27.2	.1254	15.90	15.69			69	-2.63	51.8		67.0		509	443
30	18.66	27.9	.1252	16.79	15.70			70	-3.20	52.3		68.7		443	363
31	18.12	28.6	.1250	17.67	15.73			71	-3.80	52.8		70.3		363	270
32	17.57	29.4	.1239	18.59	15.76			72	-4.45	53.3		72.0		270	158
33	17.02	30.1	.1232	19.58	15.80			73	-5.12	53.8		73.7		158	39.9
34	16.47	30.8	.1219	20.50	15.85										
35	15.93	31.5	.1207	21.50	15.91										
36	15.39	32.2	.1200	22.50	15.98										
37	14.86	32.9	.0961	23.55	17.10		39.1								
38	14.36	33.6	.0968	24.60	17.07	39.1	77.6								
39	13.85	34.2	.0970	25.65	17.05	77.6	115.5								
40	13.35	34.9	.0970	26.75	17.05	115.5	152.8								

TABLE IV. - Concluded.

(b) Assuming a minimum Inconel-718 structural ribbon thickness of 0.0248 centimeter

Turn	Magnetic field, T	Average turn diameter, cm	Thickness of Inconel 718 structural ribbon, cm	Length of aluminum conductor, m	Overall current density, kA/cm^2	Force received by turn, kN	Force passed by turn, kN
1	35.22	8.24	0.0696	0.244	18.59	0	0
2	34.63	8.84	.0736	.549	18.36		
3	34.03	9.44	.0772	.824	18.13		
4	33.43	10.05	.0810	1.159	17.93		
5	32.83	10.69	.0843	1.495	17.73		
6	32.23	11.31	.0878	1.830	17.54		
7	31.62	11.97	.0909	2.230	17.37		
8	31.01	12.62	.0942	2.625	17.20		
9	30.40	13.29	.0970	3.02	17.05		
10	29.79	13.95	.0998	3.48	16.91		
11	29.18	14.60	.1022	3.94	16.78		
12	28.57	15.27	.1049	4.42	16.65		
13	27.96	15.95	.1072	4.91	16.54		
14	27.35	16.65	.1093	5.42	16.44		
15	26.74	17.33	.1112	5.96	16.34		
16	26.15	18.01	.1132	6.56	16.25		
17	25.61	18.71	.1150	7.14	16.17		
18	25.06	19.39	.1169	7.75	16.09		
19	24.51	20.10	.1183	8.39	16.01		
20	23.97	20.80	.1198	9.02	15.95		
21	23.42	21.50	.1210	9.70	15.89		
22	22.88	22.20	.1222	10.40	15.84		
23	22.34	22.90	.1231	11.22	15.80		
24	21.80	23.60	.1238	11.84	15.77		
25	21.27	24.35	.1243	12.60	15.74		
26	20.73	25.05	.1250	13.41	15.72		
27	20.20	25.8	.1252	14.22	15.71		
28	19.67	26.5	.1252	15.02	15.71		
29	19.14	27.2	.1252	15.90	15.71		
30	18.61	27.9	.1250	16.79	15.72		
31	18.07	28.6	.1243	17.67	15.74		
32	17.52	29.4	.1239	18.59	15.78	V	V
33	16.97	30.1	.1004	19.53	16.87		40.8
34	16.46	30.7	.1020	20.50	16.80	40.8	81.2
35	15.95	31.4	.1031	21.5	16.74	81.2	121.2
36	15.44	32.1	.1040	22.5	16.69	121.2	156.5
37	14.92	32.8	.1049	23.5	16.65	156.5	200.0
38	14.41	33.4	.1058	24.6	16.62	200.0	239
39	13.89	34.1	.1060	25.6	16.60	239	276
40	13.38	34.8	.1061	27.7	16.59	276	314
41	12.86	35.4	0.1060	27.8	16.60	314	350
42	12.35	36.2	.1058	29.9	16.61	350	386
43	11.83	36.8	.1052	30.1	16.64	386	421
44	11.32	37.4	.1020	31.3	16.68	421	455
45	10.81	38.2	.1034	32.5	16.74	455	487
46	10.27	38.3	.1015	33.75	16.82	487	519
47	9.68	39.5	.0990	35.0	16.95	519	550
48	9.10	40.2	.0962	36.3	17.09	550	580
49	8.53	40.8	.0932	37.6	17.25	580	602
50	7.96	41.4	.0899	38.85	17.43	602	634
51	7.40	42.1	.0861	40.1	17.63	634	659
52	6.84	42.8	.0820	41.2	17.86	659	682
53	6.29	43.4	.0777	42.9	18.11	682	704
54	5.74	44.0	.0729	44.3	18.39	704	723
55	5.20	44.6	.0681	45.6	18.70	723	738
56	4.67	45.2	.0627	47.1	19.03	738	759
57	4.15	45.9	.0571	48.6	19.40	759	775
58	3.63	46.4	.0513	49.9	19.80	775	789
59	3.12	47.0	.0451	51.4	20.23	789	779
60	2.64	47.5	.0391	52.9	20.68	778	811
61	2.10	48.1	.0318	54.4	21.25	811	818
62	1.49	48.6	.0248	56.0	21.81	818	821
63	.91	49.1		57.5		821	815
64	.33	49.6		59.0		815	797
65	-.26	50.1		60.6		797	767
66	-.84	50.6		62.2		767	726
67	-1.42	51.1		63.9		726	674
68	-2.00	51.6		65.5		674	608
69	-2.58	52.1		67.2		608	531
70	-3.15	52.6		68.9		531	441
71	-3.74	53.3		70.5		441	339
72	-4.38	53.7		72.3		339	222
73	-5.06	54.2	V	74.0	V	222	90

TABLE V. - MAGNETIC FIELDS FOR FINAL MAGNET DESIGN

(a) Axial

Turn	Distance from centerline, cm	Distance from center plane, m: 0	0.02	0.04	0.06	0.08	0.10	0.12	0.14	0.16
		Magnetic field, T								
0	0.	32.451	32.711	32.974	32.606	31.521	29.759	27.104	23.541	19.681
1	4.113	31.157	32.642	33.487	33.104	31.499	30.448	27.946	23.803	18.886
2	4.416	30.655	32.081	32.877	32.495	31.068	29.862	27.391	23.367	18.724
3	4.722	30.513	31.545	32.268	31.887	30.566	29.279	26.842	22.959	18.543
4	5.033	30.135	31.019	31.666	31.285	30.035	28.704	26.303	22.563	18.344
5	5.347	29.729	30.497	31.069	30.688	29.490	28.135	25.774	22.172	18.131
6	5.665	29.298	29.975	30.476	30.094	28.936	27.571	25.254	21.782	17.904
7	5.986	28.848	29.449	29.886	29.502	28.377	27.012	24.740	21.394	17.666
8	6.310	28.383	28.921	29.300	28.913	27.816	26.457	24.233	21.006	17.419
9	6.637	27.905	28.389	28.716	28.326	27.255	25.906	23.731	20.617	17.163
10	6.967	27.417	27.854	28.133	27.741	26.693	25.358	23.233	20.228	16.901
11	7.300	26.922	27.316	27.552	27.157	26.133	24.813	22.739	19.839	16.633
12	7.636	26.421	26.774	26.971	26.574	25.574	24.271	22.247	19.449	16.361
13	7.974	25.917	26.229	26.391	25.993	25.018	23.731	21.758	19.058	16.085
14	8.315	25.413	25.681	25.811	25.412	24.466	23.193	21.270	18.665	15.805
15	8.657	24.909	25.129	25.231	24.834	23.924	22.659	20.785	18.270	15.524
16	9.002	24.398	24.601	24.685	24.289	23.401	22.159	20.333	17.897	15.241
17	9.348	23.894	24.105	24.177	23.784	22.900	21.699	19.921	17.552	14.957
18	9.697	23.390	23.604	23.670	23.280	22.408	21.242	19.511	17.203	14.672
19	10.047	22.889	23.102	23.163	22.778	21.921	20.787	19.102	16.853	14.385
20	10.399	22.387	22.598	22.657	22.277	21.438	20.333	18.693	16.503	14.098
21	10.752	21.887	22.094	22.151	21.778	20.958	19.883	18.286	16.153	13.809
22	11.106	21.386	21.590	21.646	21.281	20.480	19.434	17.881	15.802	13.519
23	11.462	20.886	21.087	21.143	20.786	20.005	18.988	17.477	15.452	13.227
24	11.818	20.385	20.583	20.640	20.293	19.533	18.544	17.075	15.102	12.935
25	12.176	19.884	20.081	20.140	19.803	19.063	18.103	16.674	14.753	12.641
26	12.534	19.383	19.579	19.641	19.314	18.595	17.664	16.276	14.405	12.346
27	12.892	18.882	19.078	19.145	18.829	18.129	17.229	15.881	14.057	12.050
28	13.250	18.379	18.579	18.650	18.346	17.666	16.796	15.488	13.711	11.753
29	13.609	17.876	18.081	18.158	17.865	17.203	16.366	15.097	13.366	11.455
30	13.968	17.372	17.587	17.670	17.389	16.740	15.940	14.711	13.025	11.155
31	14.326	16.866	17.080	17.166	16.898	16.271	15.500	14.310	12.672	10.855
32	14.684	16.358	16.558	16.646	16.391	15.795	15.044	13.892	12.306	10.553
33	15.041	15.851	16.042	16.132	15.889	15.319	14.593	13.480	11.946	10.251
34	15.398	15.342	15.528	15.620	15.391	14.845	14.146	13.071	11.587	9.948
35	15.753	14.834	15.016	15.112	14.895	14.373	13.701	12.666	11.231	9.645
36	16.107	14.326	14.507	14.607	14.404	13.904	13.261	12.264	10.876	9.342
37	16.459	13.819	14.000	14.106	13.916	13.438	12.824	11.866	10.524	9.040
38	16.788	13.344	13.526	13.639	13.461	13.003	12.418	11.496	10.196	8.756
39	17.116	12.865	13.052	13.173	13.007	12.568	12.012	11.127	9.868	8.471
40	17.448	12.385	12.577	12.708	12.553	12.133	11.607	10.760	9.540	8.184
41	17.774	11.901	12.102	12.244	12.101	11.698	11.204	10.394	9.213	7.896
42	18.098	11.414	11.627	11.781	11.649	11.262	10.801	10.031	8.886	7.606
43	18.438	10.922	11.153	11.319	11.197	10.823	10.399	9.668	8.560	7.315
44	18.769	10.427	10.680	10.859	10.746	10.380	9.998	9.308	8.236	7.021
45	19.096	9.926	10.224	10.412	10.309	9.931	9.611	8.962	7.928	6.726
46	19.424	9.419	9.721	9.911	9.818	9.456	9.169	8.561	7.578	6.429
47	19.750	8.909	9.164	9.351	9.266	8.956	8.666	8.102	7.183	6.131
48	20.074	8.396	8.627	8.808	8.731	8.452	8.180	7.659	6.805	5.832
49	20.395	7.881	8.097	8.270	8.201	7.945	7.698	7.221	6.433	5.534
50	20.714	7.367	7.570	7.737	7.673	7.439	7.218	6.787	6.063	5.236
51	21.029	6.854	7.049	7.209	7.150	6.935	6.742	6.358	5.697	4.941
52	21.341	6.343	6.533	6.687	6.632	6.434	6.271	5.933	5.335	4.647
53	21.649	5.836	6.023	6.172	6.119	5.936	5.804	5.514	4.978	4.356
54	21.953	5.332	5.519	5.664	5.611	5.442	5.341	5.100	4.625	4.068
55	22.252	4.833	5.023	5.163	5.109	4.951	4.883	4.691	4.276	3.784
56	22.547	4.339	4.534	4.668	4.612	4.462	4.429	4.286	3.932	3.503
57	22.837	3.849	4.053	4.180	4.120	3.976	3.979	3.886	3.593	3.225
58	23.123	3.364	3.582	3.698	3.634	3.490	3.533	3.490	3.260	2.953
59	23.402	2.885	3.132	3.233	3.164	3.005	3.101	3.108	2.943	2.684
60	23.676	2.411	2.717	2.794	2.719	2.516	2.693	2.749	2.652	2.420
61	23.945	1.944	2.230	2.270	2.191	1.995	2.199	2.303	2.298	2.162
62	24.207	1.487	1.659	1.648	1.564	1.441	1.604	1.755	1.866	1.910
63	24.463	1.045	1.123	1.053	0.964	0.891	1.035	1.230	1.462	1.668
64	24.716	0.618	0.617	0.484	0.391	0.352	0.489	0.727	1.080	1.436
65	24.952	0.196	0.116	-0.088	-0.183	-0.191	-0.059	0.221	0.699	1.207
66	25.197	-0.218	-0.384	-0.663	-0.761	-0.736	-0.611	-0.292	0.317	0.982
67	25.443	-0.621	-0.882	-1.242	-1.341	-1.281	-1.168	-0.810	-0.066	0.764
68	25.688	-1.010	-1.377	-1.822	-1.921	-1.820	-1.725	-1.333	-0.449	0.553
69	25.934	-1.380	-1.870	-2.402	-2.500	-2.350	-2.284	-1.858	-0.833	0.352
70	26.180	-1.727	-2.368	-2.988	-3.084	-2.866	-2.848	-2.392	-1.222	0.161
71	26.425	-2.046	-2.897	-3.603	-3.697	-3.370	-3.442	-2.959	-1.638	-0.016
72	26.671	-2.333	-3.513	-4.298	-4.390	-3.860	-4.117	-3.611	-2.130	-0.179
73	26.916	-2.585	-4.183	-5.025	-5.114	-4.288	-4.824	-4.297	-2.675	-0.326

TABLE V. - Concluded.

(b) Radial

Turn	Distance from centerline, cm	Distance from center plane, m								
		0	0.02	0.04	0.06	0.08	0.10	0.12	0.14	0.16
		Magnetic field, T								
0	0.	0.	0.	0.	0.	0.	0.	0.	0.	0.
1	4.113	-0.000	-1.182	-0.119	0.881	1.225	2.055	3.303	4.843	3.989
2	4.416	-0.000	-1.356	-0.132	0.955	1.276	2.185	3.538	5.300	4.279
3	4.722	0.000	-1.492	-0.144	1.027	1.354	2.317	3.769	5.692	4.563
4	5.033	0.000	-1.596	-0.153	1.096	1.442	2.449	3.994	6.040	4.839
5	5.347	-0.000	-1.675	-0.158	1.161	1.532	2.583	4.213	6.354	5.105
6	5.666	-0.000	-1.735	-0.159	1.223	1.624	2.717	4.424	6.643	5.360
7	5.986	0.000	-1.779	-0.157	1.282	1.716	2.851	4.628	6.910	5.604
8	6.310	0.000	-1.811	-0.151	1.339	1.807	2.985	4.825	7.159	5.836
9	6.637	-0.000	-1.833	-0.141	1.395	1.897	3.116	5.013	7.391	6.058
10	6.967	0.000	-1.847	-0.129	1.449	1.986	3.246	5.194	7.610	6.270
11	7.300	-0.000	-1.853	-0.113	1.502	2.074	3.374	5.367	7.814	6.471
12	7.636	-0.000	-1.854	-0.095	1.553	2.160	3.499	5.532	8.005	6.663
13	7.974	-0.000	-1.848	-0.074	1.604	2.245	3.621	5.690	8.184	6.845
14	8.315	-0.000	-1.836	-0.052	1.653	2.329	3.740	5.841	8.349	7.018
15	8.657	0.000	-1.818	-0.029	1.700	2.413	3.855	5.985	8.499	7.183
16	9.002	-0.000	-1.797	-0.005	1.747	2.499	3.966	6.122	8.635	7.340
17	9.349	0.000	-1.776	0.020	1.793	2.579	4.074	6.254	8.769	7.490
18	9.697	-0.000	-1.759	0.045	1.838	2.653	4.177	6.380	8.903	7.634
19	10.047	0.000	-1.744	0.069	1.882	2.725	4.276	6.501	9.034	7.771
20	10.399	-0.000	-1.731	0.093	1.926	2.793	4.371	6.617	9.161	7.903
21	10.752	0.000	-1.719	0.117	1.968	2.859	4.462	6.728	9.284	8.030
22	11.106	0.000	-1.710	0.139	2.008	2.922	4.549	6.834	9.402	8.151
23	11.462	0.000	-1.701	0.161	2.048	2.982	4.631	6.935	9.517	8.267
24	11.818	0.000	-1.694	0.181	2.085	3.040	4.709	7.032	9.626	8.378
25	12.176	-0.000	-1.688	0.200	2.121	3.094	4.783	7.124	9.731	8.484
26	12.534	0.000	-1.684	0.217	2.155	3.146	4.853	7.211	9.832	8.585
27	12.892	0.000	-1.681	0.233	2.188	3.194	4.918	7.294	9.929	8.681
28	13.253	-0.000	-1.681	0.248	2.218	3.240	4.980	7.373	10.022	8.772
29	13.609	0.000	-1.682	0.260	2.247	3.282	5.037	7.447	10.112	8.859
30	13.968	0.000	-1.687	0.272	2.273	3.319	5.090	7.516	10.200	8.940
31	14.325	-0.000	-1.693	0.282	2.297	3.352	5.139	7.581	10.286	9.016
32	14.684	0.000	-1.700	0.290	2.319	3.383	5.183	7.641	10.364	9.086
33	15.041	-0.000	-1.705	0.297	2.339	3.412	5.224	7.696	10.433	9.151
34	15.398	0.000	-1.710	0.302	2.356	3.439	5.261	7.747	10.496	9.211
35	15.755	0.000	-1.714	0.306	2.370	3.463	5.294	7.792	10.552	9.265
36	16.107	-0.000	-1.719	0.309	2.382	3.483	5.322	7.833	10.602	9.313
37	16.459	0.000	-1.725	0.310	2.393	3.501	5.347	7.869	10.648	9.356
38	16.758	-0.000	-1.732	0.309	2.400	3.514	5.366	7.898	10.686	9.392
39	17.114	-0.000	-1.740	0.307	2.406	3.525	5.381	7.923	10.721	9.424
40	17.448	-0.000	-1.750	0.304	2.410	3.533	5.392	7.945	10.752	9.451
41	17.773	0.000	-1.763	0.299	2.413	3.538	5.400	7.962	10.780	9.474
42	18.108	0.000	-1.778	0.293	2.415	3.540	5.403	7.975	10.806	9.492
43	18.438	0.000	-1.797	0.285	2.415	3.539	5.402	7.984	10.830	9.506
44	18.768	0.000	-1.821	0.276	2.414	3.534	5.396	7.989	10.855	9.515
45	19.096	0.000	-1.850	0.267	2.412	3.523	5.386	7.988	10.883	9.519
46	19.424	0.000	-1.883	0.257	2.409	3.504	5.372	7.982	10.912	9.517
47	19.750	0.000	-1.913	0.246	2.404	3.487	5.354	7.971	10.928	9.509
48	20.074	0.000	-1.938	0.235	2.397	3.472	5.333	7.954	10.929	9.493
49	20.395	0.000	-1.958	0.224	2.389	3.455	5.307	7.932	10.917	9.471
50	20.714	0.000	-1.975	0.214	2.379	3.436	5.277	7.903	10.896	9.442
51	21.029	0.000	-1.990	0.203	2.369	3.415	5.244	7.869	10.866	9.406
52	21.341	0.000	-2.003	0.193	2.357	3.391	5.207	7.828	10.828	9.362
53	21.649	0.000	-2.016	0.184	2.345	3.366	5.166	7.782	10.784	9.312
54	21.953	-0.000	-2.028	0.176	2.333	3.339	5.121	7.730	10.732	9.255
55	22.252	0.000	-2.040	0.169	2.320	3.309	5.072	7.672	10.675	9.191
56	22.547	0.000	-2.052	0.163	2.308	3.278	5.020	7.609	10.613	9.121
57	22.837	-0.000	-2.066	0.159	2.296	3.245	4.964	7.540	10.547	9.044
58	23.123	0.000	-2.081	0.156	2.285	3.210	4.905	7.466	10.479	8.961
59	23.402	0.000	-2.099	0.156	2.274	3.171	4.844	7.386	10.411	8.872
60	23.676	0.000	-2.120	0.158	2.263	3.126	4.780	7.300	10.345	8.773
61	23.945	-0.000	-2.138	0.163	2.251	3.076	4.715	7.209	10.277	8.668
62	24.207	-0.000	-2.147	0.170	2.239	3.030	4.649	7.113	10.192	8.556
63	24.460	0.000	-2.142	0.181	2.226	2.989	4.584	7.012	10.085	8.437
64	24.706	-0.000	-2.123	0.195	2.211	2.951	4.520	6.907	9.960	8.312
65	24.952	-0.000	-2.091	0.212	2.195	2.914	4.455	6.795	9.815	8.176
66	25.197	-0.000	-2.045	0.232	2.176	2.877	4.389	6.676	9.649	8.030
67	25.443	-0.000	-1.983	0.257	2.154	2.839	4.324	6.549	9.462	7.873
68	25.688	0.000	-1.904	0.285	2.128	2.803	4.260	6.414	9.251	7.706
69	25.934	-0.000	-1.804	0.316	2.100	2.767	4.196	6.274	9.014	7.528
70	26.180	-0.000	-1.680	0.351	2.068	2.735	4.133	6.127	8.745	7.340
71	26.425	0.000	-1.527	0.388	2.032	2.709	4.072	5.974	8.437	7.144
72	26.671	-0.000	-1.339	0.427	1.993	2.695	4.011	5.818	8.077	6.941
73	26.916	0.000	-1.119	0.468	1.952	2.704	3.951	5.658	7.661	6.733

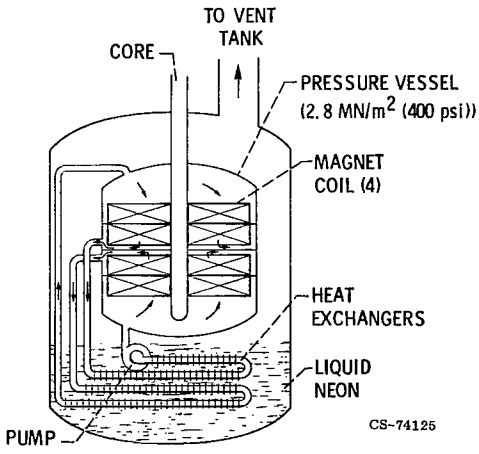

(a) Conceptual design.

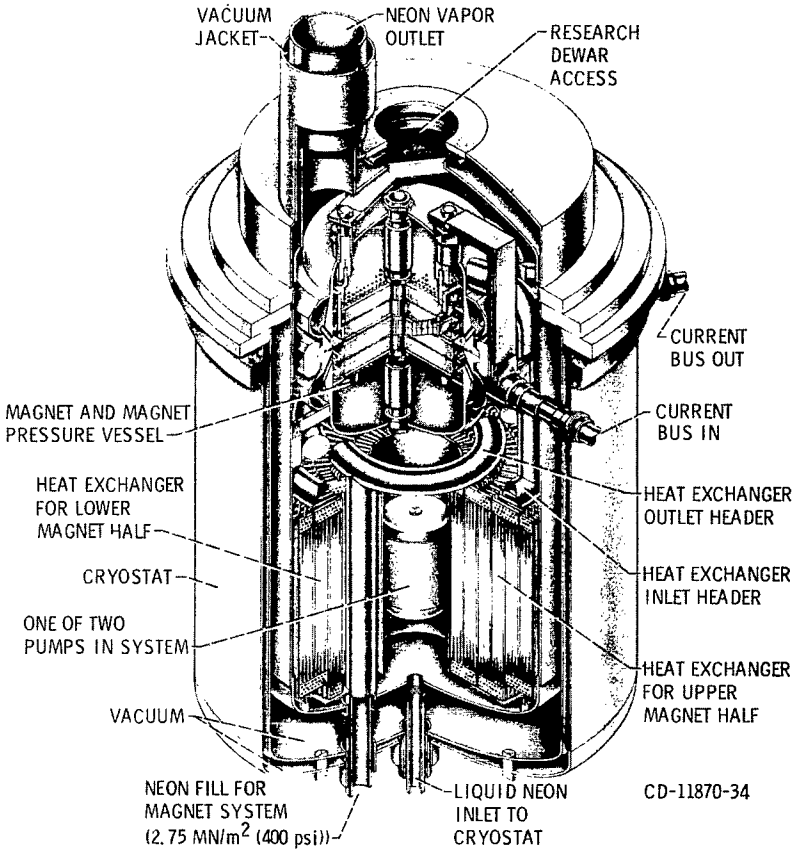

(b) Cutaway.

Figure 1. - Thirty-tesla magnet system.

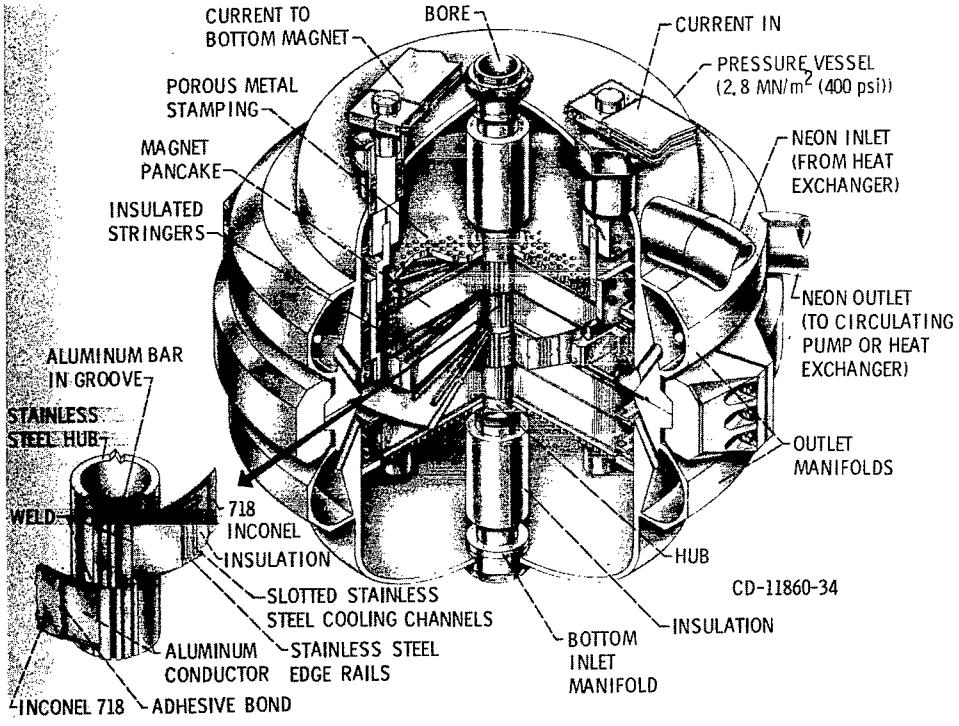

Figure 2. - Conceptual design of 30-tesla, liquid-cooled magnet (entire system enclosed in cryostat).

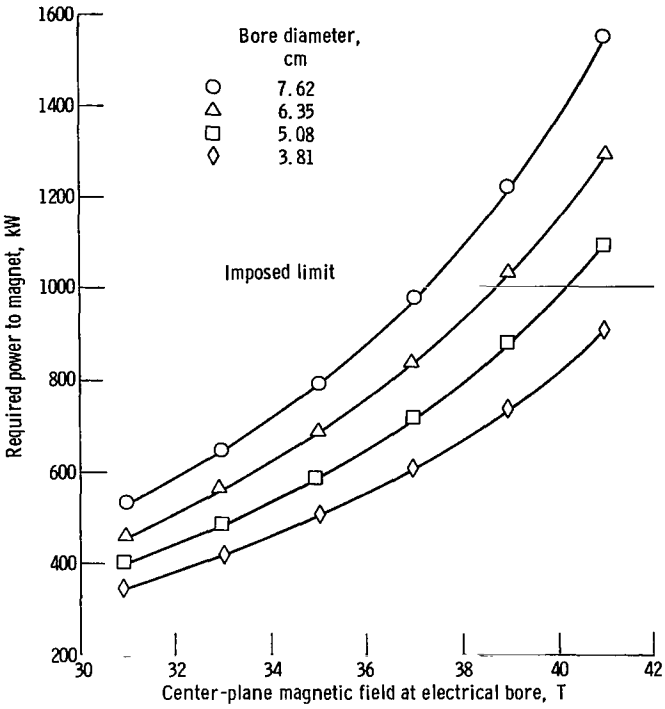

Figure 3. - Power required to reach various magnetic fields for different bore diameters. (Heat flux varied from 9.98 W/cm^2 at 31 T to 10.46 W/cm^2 at 41 T.)

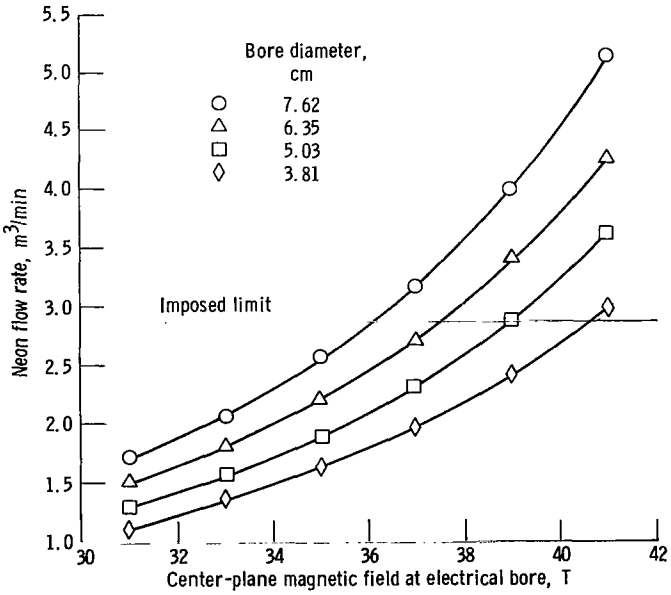

Figure 4. - Neon flow rate required to maintain 5-kelvin temperature rise at various magnetic fields and bore diameters.

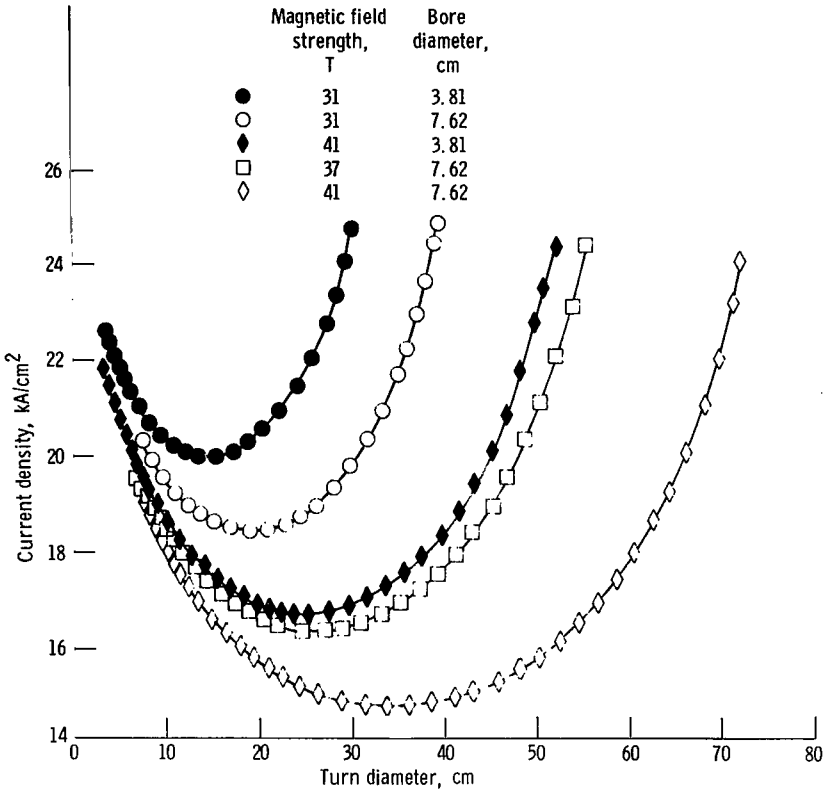

Figure 5. - Current density as function of turn diameter for various design magnetic field strengths and bore diameters. Conductor width, 5.71 centimeters.

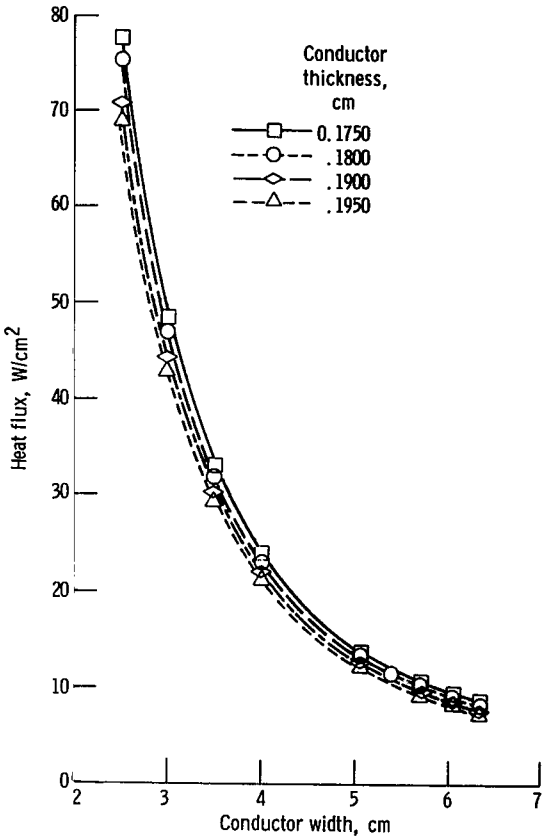

Figure 6. - Heat flux as function of conductor width for various conductor thicknesses and a fixed current of 40 kiloamperes.

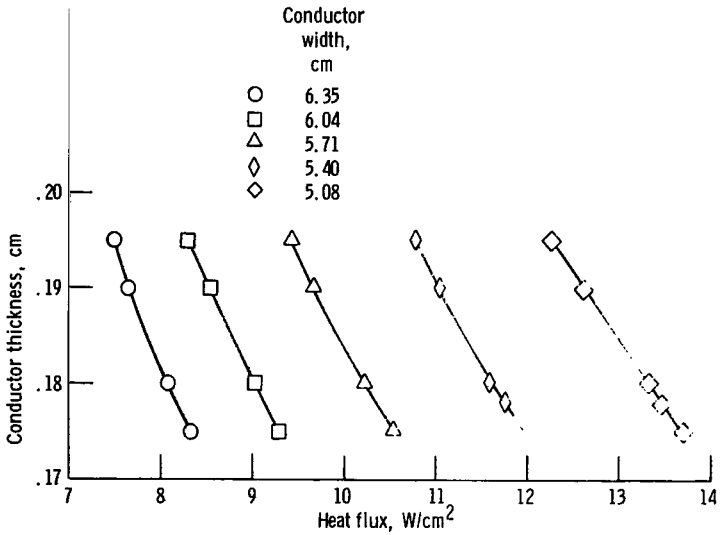

Figure 7. - Heat flux as function of conductor thickness for various conductor widths and a fixed current of 40 kiloamperes.

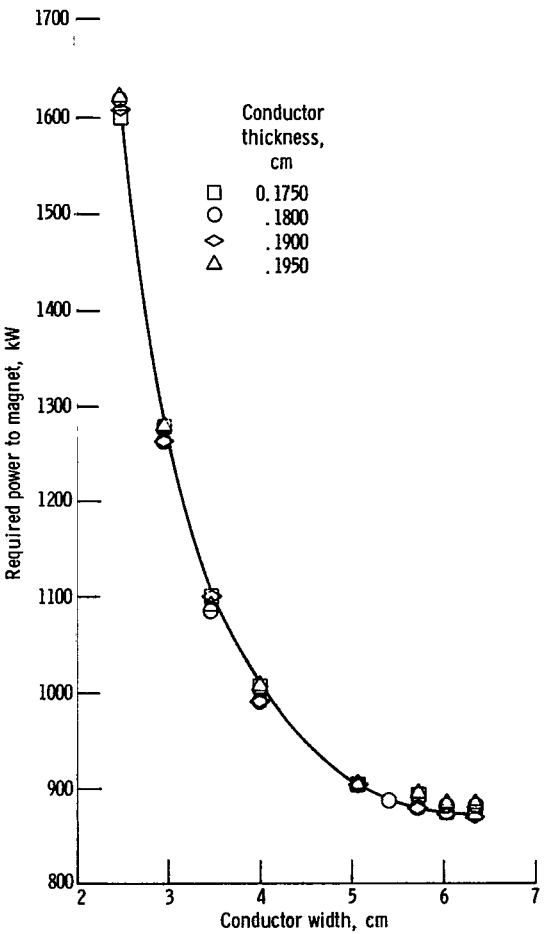

Figure 8. - Magnet power required as function of conductor width and thickness.

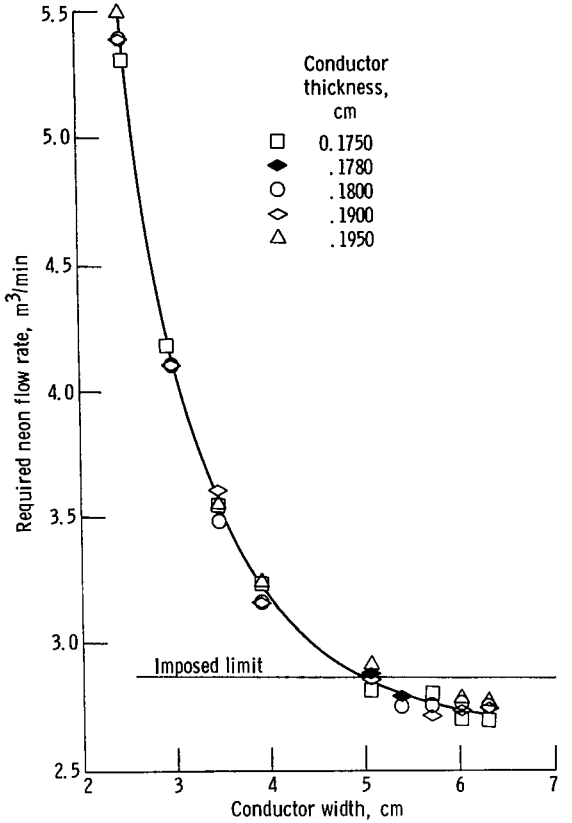

Figure 9. - Required neon flow rate as function of conductor width and thickness.

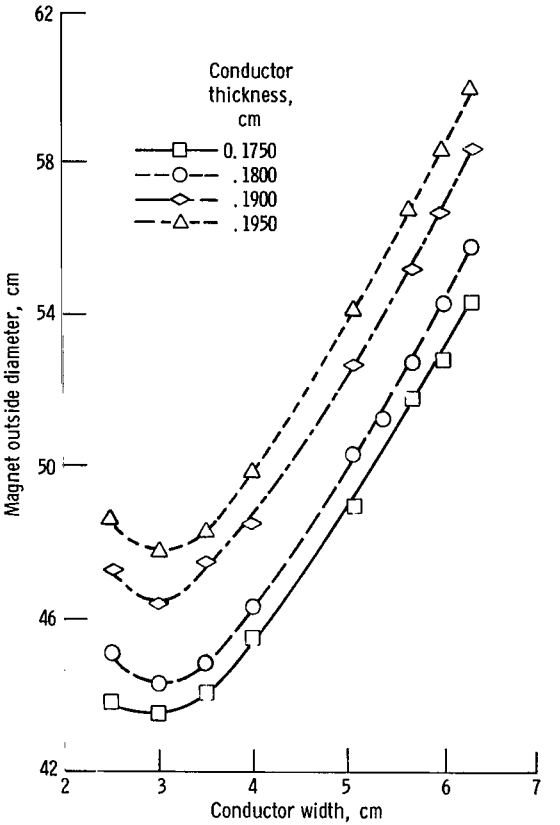

Figure 10. - Magnet outside diameter as function of conductor width and thickness.

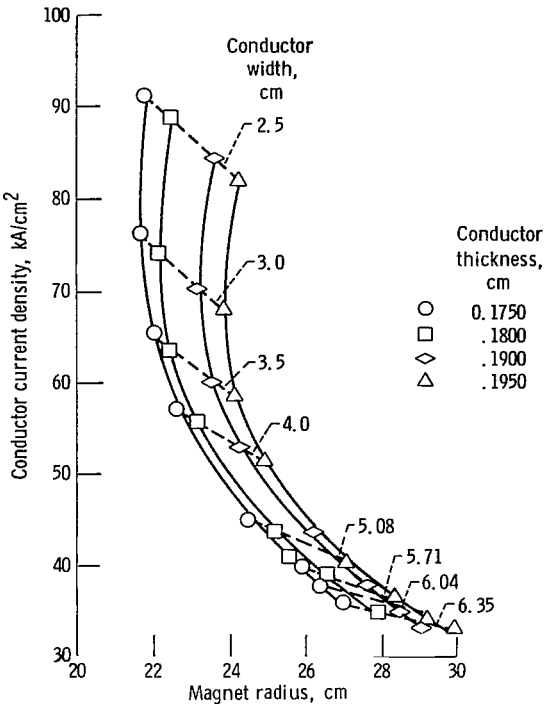

Figure 11. - Current density as function of magnet radius for various conductor thicknesses.

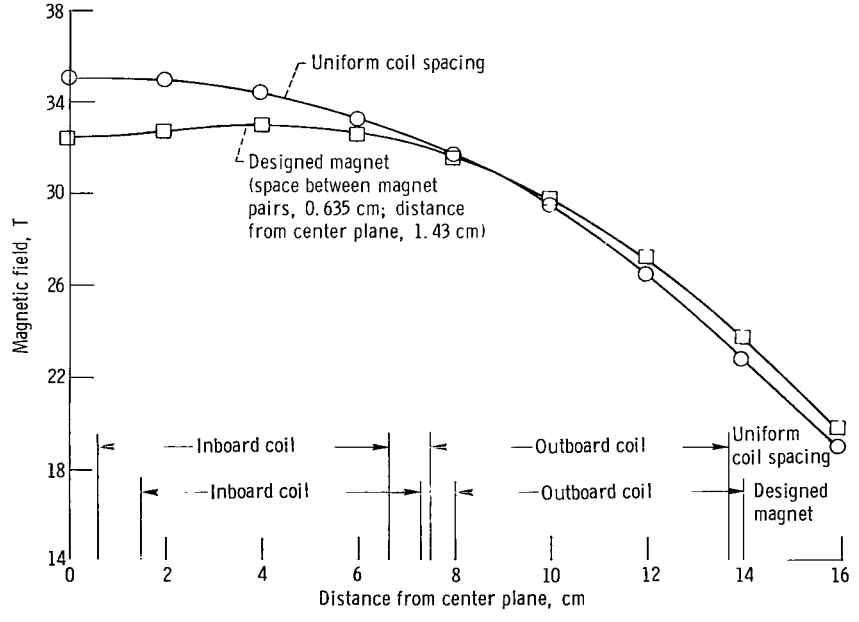

Figure 12. - Comparison of magnetic field along axis for uniform coil spacing and for designed magnet. Axial packing fraction, 0.85 in both cases.

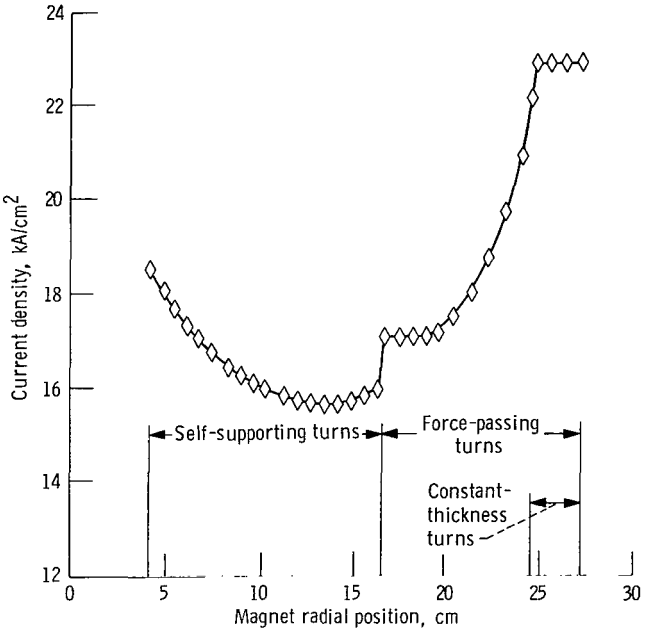

Figure 13. - Total local average current density as function of radial position.

"The aeronautical and space activities of the United States shall be conducted so as to contribute . . . to the expansion of human knowledge of phenomena in the atmosphere and space. The Administration shall provide for the widest practicable and appropriate dissemination of information concerning its activities and the results thereof."

—NATIONAL AERONAUTICS AND SPACE ACT OF 1958

NASA SCIENTIFIC AND TECHNICAL PUBLICATIONS

TECHNICAL REPORTS: Scientific and technical information considered important, complete, and a lasting contribution to existing knowledge.

TECHNICAL NOTES: Information less broad in scope but nevertheless of importance as a contribution to existing knowledge.

TECHNICAL MEMORANDUMS: Information receiving limited distribution because of preliminary data, security classification, or other reasons. Also includes conference proceedings with either limited or unlimited distribution.

CONTRACTOR REPORTS: Scientific and technical information generated under a NASA contract or grant and considered an important contribution to existing knowledge.

TECHNICAL TRANSLATIONS: Information published in a foreign language considered to merit NASA distribution in English.

SPECIAL PUBLICATIONS: Information derived from or of value to NASA activities. Publications include final reports of major projects, monographs, data compilations, handbooks, sourcebooks, and special bibliographies.

TECHNOLOGY UTILIZATION PUBLICATIONS: Information on technology used by NASA that may be of particular interest in commercial and other non-aerospace applications. Publications include Tech Briefs, Technology Utilization Reports and Technology Surveys.

Details on the availability of these publications may be obtained from:

SCIENTIFIC AND TECHNICAL INFORMATION OFFICE

NATIONAL AERONAUTICS AND SPACE ADMINISTRATION

Washington, D.C. 20546